SCIENTIFIC REPORTS

OPEN

Superamphiphobic Cu/CuO Micropillar Arrays with High Repellency Towards Liquids of Extremely High Viscosity and Low Surface Tension

Received: 5 September 2018
Accepted: 6 December 2018
Published online: 24 January 2019

Qing Zhu[1], Bucheng Li[2], Shangbin Li[1], Guan Luo[1], Baohui Zheng[1] & Junping Zhang[2]

For almost all the research of super anti-wetting surfaces, pure liquids like water and *n*-hexadecane are used as the probes. However, liquids of diverse compositions are used in academic research, industrial production and our daily life. Obviously, the liquid repellency of super anti-wetting coatings is highly dependent on properties of the liquids. Here, we report the first superamphiphobic surface with high repellency towards liquids of extremely high viscosity and low surface tension. The surfaces were prepared by constructing a hierarchical micro-/nanostructure on the Cu micropillar arrays followed by modification with perfluorosilane. The surfaces are superamphiphobic towards the liquids with extremely high viscosity and low surface tension because of (i) the micro-/nanostructured surface composed of micropillars with proper pillar distance and CuO nano-flowers, and (ii) the abundant perfluorodecyl groups on the surface. The contact angles, sliding angles, apparent contact line at the solid-liquid interface and adhesion forces are the end products of micropillar distance, viscosity and surface tension. Smaller micropillar distance, higher viscosity and higher surface tension contribute to reducing the adhesion force. We *in situ* observed the process of microcapillary bridge rupture for the first time using highly viscous liquids. We also successfully reduced the adhesion forces and enhanced the average rolling velocity of liquids with extremely high viscosity and low surface tension by regulating the micropillar distance.

Inspired by the unique wettability of the lotus leaf[1,2], artificial super anti-wetting surfaces such as superhydrophobic[3–5] and superamphiphobic surfaces[6–8] have generated great attention in academia and industry. Super anti-wetting surfaces have wide potential applications in many fields including self-cleaning surfaces[9], oil/water separation[10,11], anti-corrosion[12,13], anti-icing[14,15] and anti-wetting textiles[16,17]. Thus, a wide range of methods and materials have been used to prepare super anti-wetting surfaces[18–23]. More specifically, to understand the solid-liquid interaction (e.g., impinging/bouncing[24–26], sliding[27] and modeling/simulation[28,29]) and to move the surfaces to real world applications (e.g., enhancing mechanical stability[30–32], enhancing transparency[33,34], waterborne[35,36], flexible[37,38] and applications[39–42]) are now in the spotlights in the field of super anti-wetting surfaces.

For all the fundamental and applied research of super anti-wetting surfaces, the repellency of the surfaces to liquids is crucial. While most of the attention has been being paid to the surfaces, the liquids as the counterparts are neglected[43]. In most cases, researchers simply used pure liquids like water (for superhydrophobic surfaces) and *n*-hexadecane (for superamphiphobic surfaces) as the probes. Obviously, the liquid repellency of super anti-wetting coatings is highly dependent on properties of the liquids[25,44–46]. For anti-icing, the interaction between superhydrophobic surfaces and super-cooled water is very different from that at room temperature because of high viscosity of super-cooled water[25,47]. The viscosity of water at −30 °C is ca. 5 times higher than that

[1]Institute of Chemical Materials, China Academy of Engineering Physics, 621999, Mianyang, P. R. China. [2]Key Laboratory of Clay Mineral Applied Research of Gansu Province, Lanzhou Institute of Chemical Physics, Chinese Academy of Sciences, 730000, Lanzhou, P. R. China. Qing Zhu and Bucheng Li contributed equally. Correspondence and requests for materials should be addressed to S.L. (email: caeplisb@163.com) or J.Z. (email: jpzhang@licp.cas.cn)

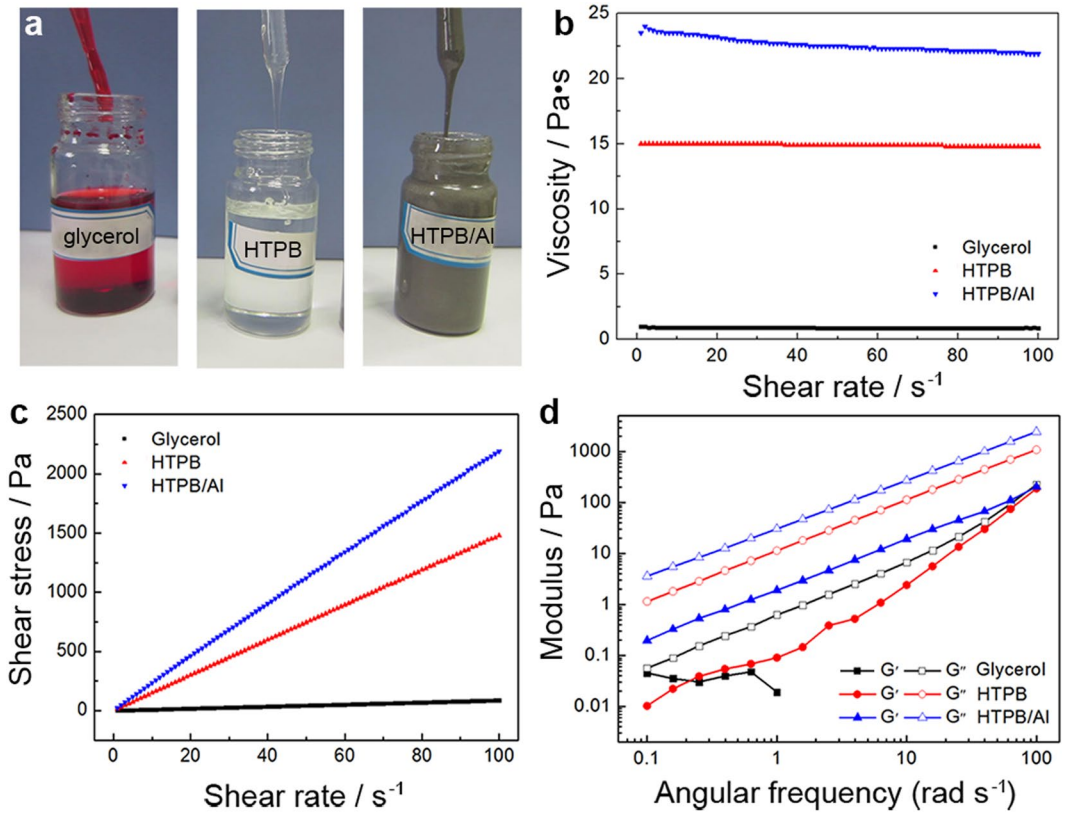

Figure 1. Properties of probing liquids. (**a**) Photographs of glycerol, HTPB and HTPB/Al. (**b**,**c**) Steady and (**c**) dynamic rheological behavior of glycerol, HTPB and HTPB/Al.

at room conditions. For superamphiphobic surfaces, pure liquids with different surface tensions ranging from 72.8 mN m^{-1} (water) to 22.5 mN m^{-1} (methanol) were studied.

However, liquids of diverse compositions, e.g., solutions, suspensions and emulsions, are used in academic research, industrial production and our daily life. The properties of these liquids including viscosity, surface tension, density and flow form are far different from those of the frequently used pure liquids in the field of super anti-wetting surfaces. Consequently, the solid-liquid interaction and liquid repellency will be changed evidently, which requires design of novel surface microstructures. Nevertheless, the research about super anti-wetting coatings repelling complex liquids, e.g., high viscosity, high solid content and low surface tension, is very rare. Brown and Bhushan reported superoleophobic polypropylene surfaces exhibiting some repellency towards shampoos[48]. The mixtures of glycerol and water were also used as the model liquids of different viscosity ranging from 0.959 mPa·s (water) to 950 mPa·s (glycerol)[44,49]. Research about super anti-wetting coatings repelling complex liquids is of great importance for their development and applications.

Here, we report preparation of superamphiphobic surfaces with high repellency towards liquids of extremely high viscosity and low surface tension. The surfaces were prepared by constructing a hierarchical micro-/nanostructure on the Cu micropillar arrays followed by modification with perfluorosilane. Hydroxyl-terminated polybutadiene (HTPB) and the HTPB/Al mixture (1:1, w/w) were used as the probing complex liquids with high viscosity, high solid content and low surface tension. HTPB, a viscous mixture rather than a pure compound, is an oligomer of butadiene, and could react with isocyanates to form polyurethane polymers.

Results

Properties of probing liquids. HTPB and the HTPB/Al mixture (1:1) were used as the probing complex liquids with high viscosity, high solid content and low surface tension (Fig. 1a). Water and glycerol were also studied for comparison. The dynamic viscosity, surface tension and density of these liquids are listed in Table 1. The dynamic viscosity of HTPB and HTPB/Al is 15 and 24 Pa·s, respectively, which is much higher than that of glycerol, frequently used as the representative viscous liquid. For the injection of HTPB and HTPB/Al, the diameter of the needle must be big enough (outside diameter = 1.65 mm, inside diameter = 1.25 mm) because of their very high viscosity. Also, smaller drops released from the needle with a big diameter cannot be dropped onto the superamphiphobic surfaces because the liquid/needle adhesion force is much large than that between the surfaces and the liquids. Consequently, liquid drops of 20 µL were used for the measurement of contact angles (CAs) and sliding angles (SAs). In addition, the viscosity of the liquids did not show obvious change with increasing the shear rate while the shear stress increased linearly (Fig. 1b–c), indicating that these liquids are the Newtonian fluids[50]. Oscillatory measurements showed that the storage modulus (G') of the liquids is lower than the loss modulus (G") in the angular frequency of 0.1–100 rad s^{-1} (Fig. 1d), indicating a viscous response of the liquids[50].

Liquids	Dynamic viscosity/ (Pa·s, 20 °C)	Surface tension/ (mN m^{-1}, 20 °C)	Density/(g mL^{-1})
Water	0.001	72.4	1.0
Glycerol	0.9	64.1	1.28
HTPB	15	38.4	0.89
HTPB/Al (1:1)	24	42.8	1.02

Table 1. Properties of probing liquids. Dynamic viscosity, surface tension and density of the liquids employed in the experiments.

Also, the surface tension of HTPB and HTPB/Al is 38.4 and 42.8 mN m^{-1}, respectively, which is much lower than that of water and glycerol.

Preparation of superamphiphobic Cu/CuO@PFDTCS micropillar arrays. We prepared the superamphiphobic Cu/CuO@PFDTCS micropillar arrays using the Cu micropillar arrays with the same pillar size and different pillar distance (D_{pillar} = 100, 300, 400 and 500 μm, Supplementary Fig. S1). Firstly, the oxides on the surface of the Cu micropillar arrays were removed by immersion in 0.1 M HCl aqueous solution. Then, the Cu micropillar arrays with metallic gloss were oxidized in an aqueous solution containing NaOH and ammonium persulfate. In this step, the nanostructured CuO layer was formed on the Cu micropillar arrays, and the micro-/nanostructured Cu/CuO micropillar arrays were obtained (Fig. 2a). Finally, the Cu/CuO micropillar arrays were immersed in dry toluene containing *1H,1H,2H,2H*-perfluorodecyltrichlorosilane (PFDTCS). The PFDTCS molecules preferentially anchored onto the hydroxyl groups on the CuO surface[51], and the superamphiphobic Cu/CuO@PFDTCS micropillar arrays were obtained. The surface of the Cu/CuO@PFDTCS micropillar arrays (Fig. 2b) is very rough compared with the Cu micropillar arrays. This is because CuO nano-flowers resembling miniature replicas of chrysanthemums were formed on the surface of the Cu micropillar arrays (Fig. 2c,d). Modification with PFDTCS did not cause any obvious change of surface morphology[51]. Figure 3 shows the scanning electron microscopy (SEM) images of the Cu/CuO@PFDTCS micropillar arrays with larger D_{pillar}. There is no difference in the surface morphology of the samples at both low and high magnifications except for the D_{pillar}. This means the method is reproducible, and the difference in wettability of the samples is only attributed to the D_{pillar}.

The surface chemical composition of the Cu/CuO@PFDTCS micropillar arrays was studied by X-ray photoelectron spectroscopy (XPS) with the Cu micropillar arrays for comparison. The C 1s, O 1s and Cu 2p peaks were detected in the XPS spectrum of the Cu micropillar arrays (Fig. 2e). Differently, a very strong F 1s peak appeared in the XPS spectrum, and the CF_2 peak appeared in the high-resolution C 1s spectrum of the Cu/CuO@PFDTCS micropillar arrays (Fig. 2f,g), which indicate successful bonding of the PFDTCS molecules onto the CuO nano-flowers. Also, the Cu 2p peak became weak (Fig. 2f) owing to deposition of the polymerized PFDTCS layer.

Superamphiphobicity of Cu/CuO@PFDTCS micropillar arrays. All the four Cu/CuO@PFDTCS micropillar arrays with different D_{pillar} are superamphiphobic owing to the combination of the micro-/nanostructured surface and the abundant perfluorodecyl groups. The CA and SA of various typical liquids, HTPB and HTPB/Al with different surface tensions on the surface of the arrays with a D_{pillar} of 100 μm are shown in Table 2. For all of the typical liquids investigated, even 1% cetyltrimethylammonium bromide (CTAB) aqueous solution and *n*-tetradecane, high CA (>157°) and low SA (<10°) on the surface were recorded. For, silicone oil, the SA is ca. 26.1° owing to the very low surface tension. Different from the typical liquids, the HTPB and HTPB/Al drops have smaller CA. In addition, water, glycerol, HTPB and HTPB/Al drops were spherical in shape on the surface of the arrays with a D_{pillar} of 100 μm (Fig. 4a). The HTPB and HTPB/Al drops sat very well on the arrays even after being dropped onto the arrays for 10 min (Fig. 4b,c). A larger volume of HTPB formed a liquid pancake on the surface of the arrays without penetrating into the arrays (Fig. 4d). Once immersed in HTPB, a silver mirror phenomenon was observed owing to the existence of a layer of air at the solid-liquid interface (Fig. 4e)[51]. The arrays remained completely dry after taken out of HTPB (Supplementary Movie S1). These phenomena indicate that all the four liquids are in the Cassie-Baxter state on the surface of the Cu/CuO@PFDTCS micropillar arrays with a D_{pillar} of 100 μm.

The superamphiphobic Cu/CuO@PFDTCS micropillar arrays also showed good mechanical stability according to the sand abrasion test and the water jetting test (Supplementary Fig. S2). These two methods are frequently used for evaluating the mechanical stability of superhydrophobic and superamphiphobic surfaces[22,30]. For the sand abrasion test, 500 g of sea sand microparticles 100–300 μm in diameter impacted the 45° tilted surface from a height of 50 cm in about 10 min. For the water jetting tests, water jet at 50 KPa scoured the 45° tilted surface from a height of 20 cm for a period of time. The changes in the $CA_{n\text{-hexadecane}}$ and $SA_{n\text{-hexadecane}}$ after the test were recorded to evaluate the change in the superamphiphobicity and the mechanical robustness of the surface. Although the $CA_{n\text{-hexadecane}}$ and $SA_{n\text{-hexadecane}}$ of changed quickly at the beginning of the tests, the surface remained superamphiphobic after abrasion with 500 g sand microparticles or water jetting for half an hour.

The effect of the D_{pillar} on the superamphiphobicity of the Cu/CuO@PFDTCS micropillar arrays is shown in Fig. 5. As can be seen from Fig. 5a, the D_{pillar} did not have obvious influence on the CA_{water} (166.2°~167.1°), $CA_{glycerol}$ (161.6°~163.0°) and CA_{HTPB} (150.2°~151.7°). However, the $CA_{HTPB/Al}$ is a bit higher on the arrays with a D_{pillar} of 100 μm (150.4°) than those on the other arrays (147.3°~148.6°). On the other hand, the CAs decreased gradually with decreasing the surface tension from 72.4 mN m^{-1} (water) to 38.4 mN m^{-1} (HTPB). This

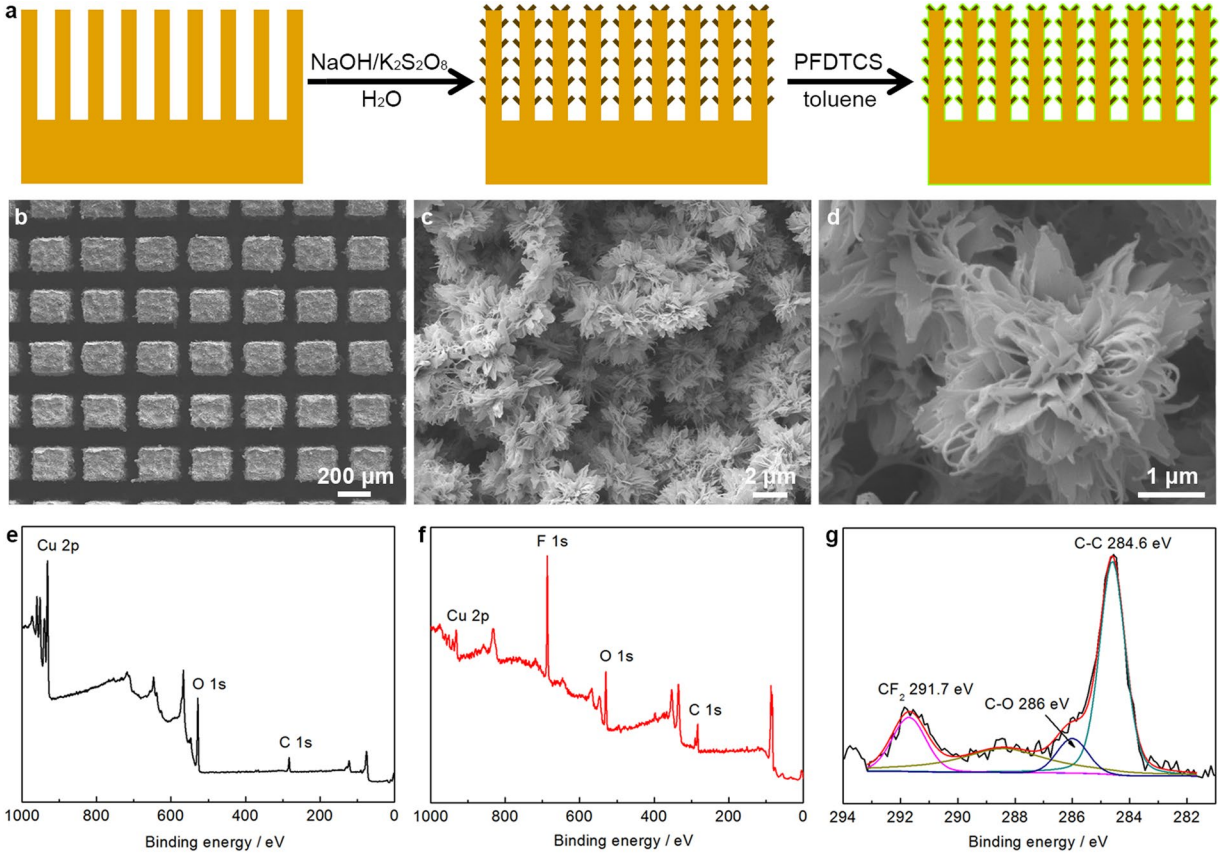

Figure 2. Preparation of superamphiphobic surfaces. (**a**) Schematic illustration of preparation of the superamphiphobic Cu/CuO@PFDTCS micropillar arrays and (**b**–**d**) their SEM images ($D_{pillar} = 100\,\mu m$). XPS spectra of (**e**) Cu micropillar arrays, (**f**) Cu/CuO@PFDTCS micropillar arrays and (**g**) high-resolution C 1s spectrum of Cu/CuO@PFDTCS micropillar arrays.

is consistent with all the literatures about superamphiphobic surfaces[6,8]. It should be noted that the $CA_{HTPB/Al}$ is slightly lower than that of the CA_{HTPB} although the surface tension of HTPB/Al (42.8 mN m^{-1}) is higher than that of HTPB. This is owing to the very high solid content of HTPB/Al.

Different from the CAs, the D_{pillar} had an evident influence on the SAs of the arrays (Fig. 5b), as the SAs are more sensitive than the CAs to the changes in microstructure and surface chemical composition of super anti-wetting surfaces[31]. All the four liquids showed much lower SAs (<6°) on the surface of the arrays with a D_{pillar} of 100 μm compared with the arrays with larger D_{pillar}. The SAs increased with increasing the D_{pillar} from 300 to 500 μm, but the difference is small. In addition, on the surface of the arrays with a D_{pillar} of 100 μm, the surface tension of the liquids showed small influence on the SAs. All the four liquids showed very low SAs, indicating high superamphiphobicity of the surface. For example, the SA_{HTPB} is 4.0° and the $SA_{HTPB/Al}$ is 5.2°. However, on the arrays with larger D_{pillar}, water has low SA, but HTPB and HTPB/Al with lower surface tension have much higher SAs. A lower SA means smaller solid-liquid interaction, and is very important for most applications of super anti-wetting surfaces.

Besides the superamphiphobic phenomena, CAs and SAs, we also analyzed the solid-liquid apparent contact line ($CL_{apparent}$) of various liquids on the surface of the Cu/CuO@PFDTCS micropillar arrays (Fig. 6a and Supplementary Fig. S3). With a D_{pillar} of 500 μm, the solid-water $CL_{apparent}$ was short, and 3 micropillars were sufficient to support a 20 μL water drop. With decreasing surface tension of the liquid to 64.1 mN m^{-1} (glycerol), the $CL_{apparent}$ suddenly increased to 4 mm (4 micropillars) because of the very big D_{pillar}. With further decreasing the surface tension and increasing the viscosity (HTPB and HTPB/Al), the $CL_{apparent}$ remained constant. This is also because of the very big D_{pillar}, and the HTPB and HTPB/Al drops cannot reach the fifth micropillar. Consequently, the micropillars supported the liquids of lower surface tension by additional contact line at the side of the micropillars, i.e., partial impalement (Fig. 6b). For the other three micropillar arrays, the $CL_{apparent}$ is the longest at a D_{pillar} of 100 μm followed by a D_{pillar} of 300 μm and 400 μm in the case of all the liquids. This means the same drop is supported by more micropillars at smaller D_{pillar}, efficiently inhibiting impalement into the spaces among the micropillars, i.e. the adhesion force on each pillar is smaller. For example, a 20 μL HTPB was supported by 9 micropillars at a D_{pillar} of 100 μm, but was only supported by 4–5 micropillars at a D_{pillar} of 300–500 μm. This should be the reason for the aforementioned increasing SAs with increasing the D_{pillar}. In addition, the micropillar arrays with a D_{pillar} of 100 μm supported various liquids very well by continuously increasing the $CL_{apparent}$ with decreasing surface tension of the liquids. However, the other arrays with higher D_{pillar} of 300 and 400 μm cannot

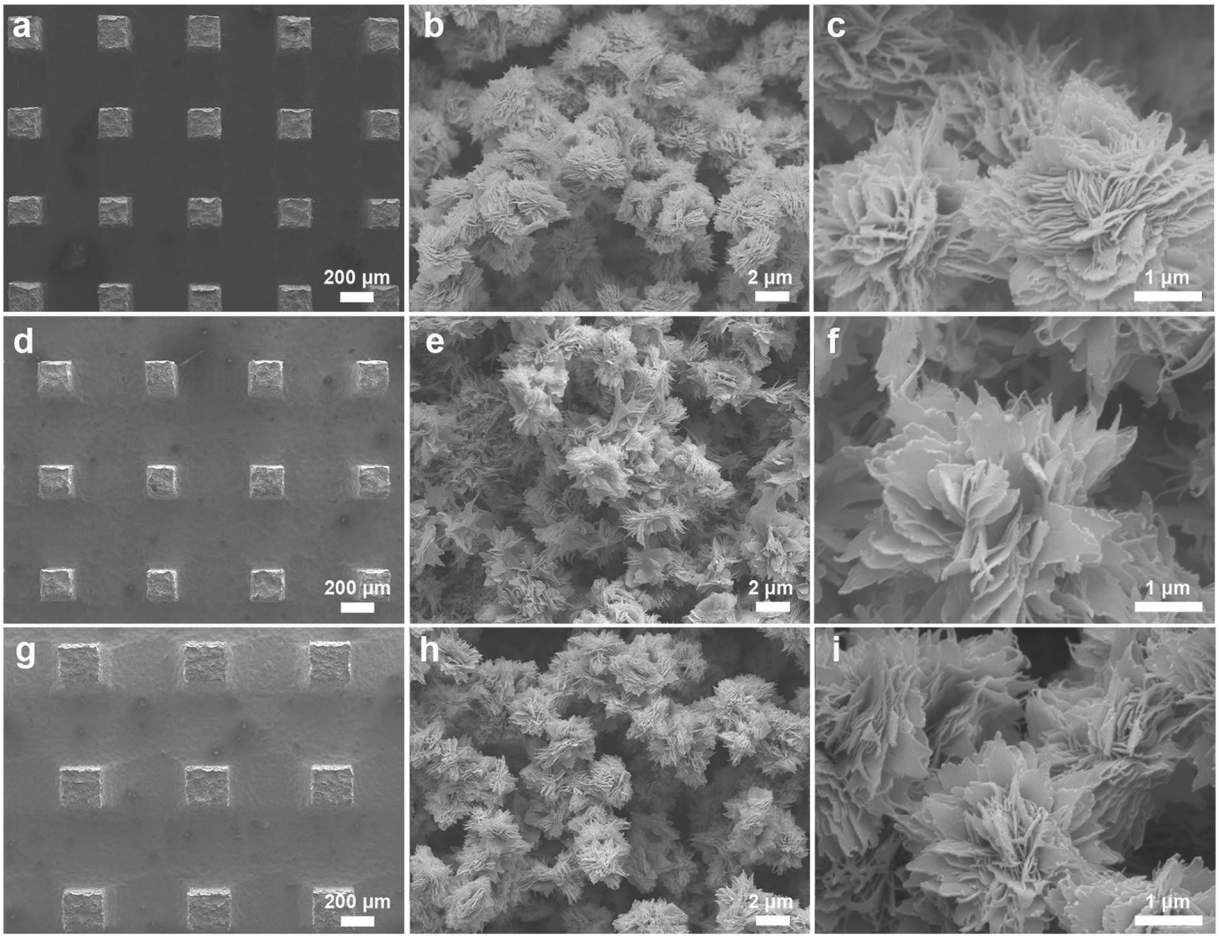

Figure 3. SEM images of Cu/CuO@PFDTCS micropillar arrays with different D_{pillar}. (**a**–**c**) 300 μm, (**d**–**f**) 400 μm and (**g**–**i**) 500 μm.

Liquids	CA/°	SA/°	Surface tension/(mN m^{-1}, 20 °C)
water	166.7	1.7	72.4
glycerol	162.9	3.7	64.1
diiodomethane	160.2	2.7	44.4
1% $CTAB_{(aq)}$	165.1	2.5	34.9
n-hexadecane	160.4	8.3	27.4
n-tetradecane	157.1	9.8	25.2
silicone oil	152.7	26.1	19.9
HTBP	151.3	4.0	38.4
HTPB/Al (1:1)	150.4	8.3	42.8

Table 2. Superamphiphobicity. CA and SA of various liquids on the surface of the Cu/CuO@PFDTCS micropillar arrays with a D_{pillar} of 100 μm.

support the liquids well enough, as the $CL_{apparent}$ remained constant with decreasing the surface tension, indicating partial impalement. Figure 6b summarized the two possible approaches that the micropillar arrays support the liquids with changing the D_{pillar} and the surface tension: i) increasing the $CL_{apparent}$, and ii) partial impalement. The Cu/CuO@PFDTCS micropillar arrays with a D_{pillar} of 100 μm can efficiently support the liquids of low surface tension without any impalement.

Kinetic interaction of Cu/CuO@PFDTCS micropillar arrays with various liquids. The kinetic interaction of the Cu/CuO@PFDTCS micropillar arrays with various liquids was studied in this section. The adhesion forces between the Cu/CuO@PFDTCS micropillar arrays and various liquids are shown in Table 3 and Supplementary Fig. S4. The D_{pillar} has a great influence on the adhesion forces. The adhesion forces of the liquids

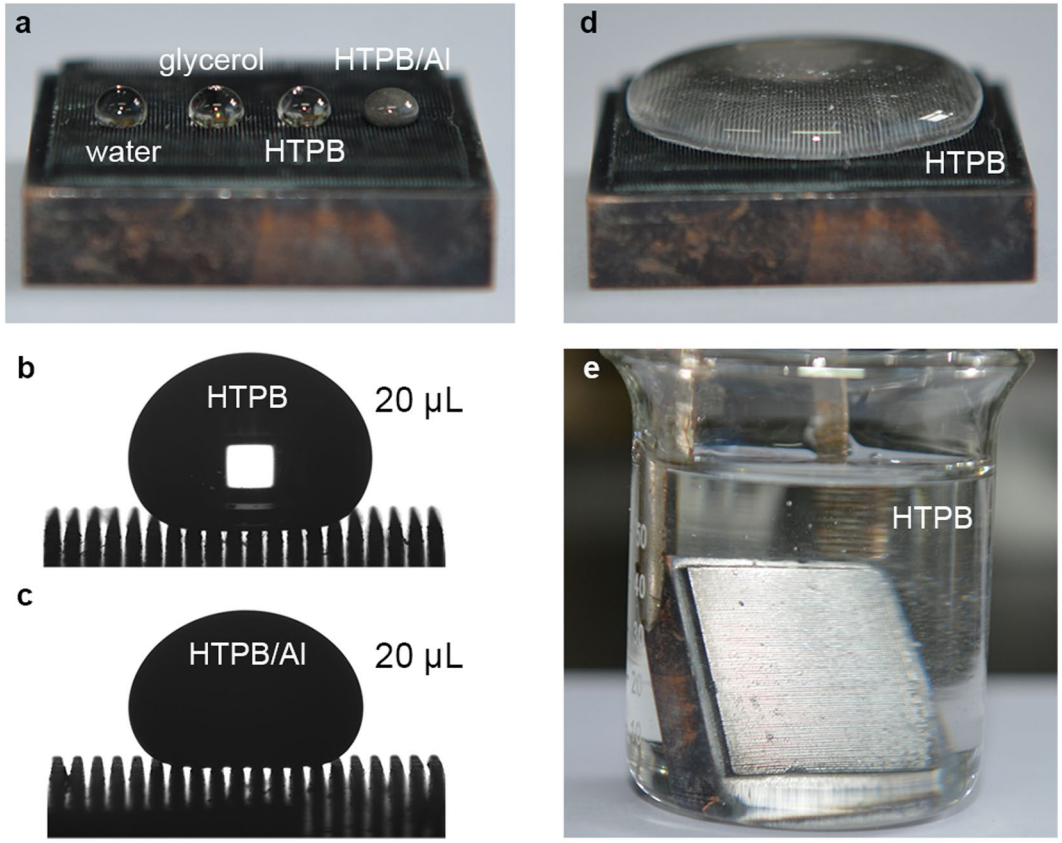

Figure 4. Photographs of the Cu/CuO@PFDTCS micropillar arrays. (**a**–**d**) with various drops and (**e**) immersed in HTPB. $D_{pillar} = 100\,\mu m$.

on the arrays with a D_{pillar} of 100 μm are much lower than those on the arrays with a D_{pillar} of 300 μm. Whereas the further increase in the D_{pillar} to 500 μm did not have obvious effect on the adhesion forces. For example, the adhesion force of HTPB on the arrays with a D_{pillar} of 100 μm is 23.6 μN, whereas the adhesion forces are in the range 69.5–75.5 μN on the arrays with D_{pillar} of 300–500 μm. In addition, it was found that the surface tension and viscosity of the liquids also have big influence on the adhesion forces. On all the arrays, the adhesion forces are in the order glycerol < water < HTPB/Al < HTPB, except for small deviation for HTPB and HTPB/Al on the arrays with a D_{pillar} of 100 μm. It is a common phenomenon that the adhesion force of glycerol is smaller than that of water regardless of the D_{pillar}. The difference in surface tension between water and glycerol is small, whereas the viscosity of glycerol is much higher than that of water. So, a higher viscosity is helpful to reduce the adhesion force for liquids of similar surface tension. Compared to water, the viscosity of HTPB is much higher (15 Pa·s *vs* 0.001 Pa·s), which is helpful to reduce the adhesion force. Meanwhile, the surface tension of HTPB is much lower (38.4 mN m^{-1} *vs* 72.4 mN m^{-1}), which tend to enhance the adhesion force[47]. Owing to the synergistic effects of viscosity and surface tension, the adhesion forces of HTPB are higher than those of water on the arrays with D_{pillar} of 300–500 μm, and the adhesion forces of HTPB and water are almost the same on the arrays with a D_{pillar} of 100 μm. This result further proves that a high viscosity of liquids can reduce the adhesion force, and compensate the effect of lower surface tension in increasing the adhesion force. For example, HTPB/Al with higher viscosity and surface tension than HTPB showed obviously lower adhesion forces on the arrays with D_{pillar} of 300–500 μm. Thus, the adhesion forces in Table 3 are the end product of D_{pillar}, viscosity and surface tension. Smaller D_{pillar}, higher viscosity and higher surface tension contribute to reducing the adhesion force.

The influences of D_{pillar}, viscosity and surface tension on the adhesion forces were also well evidenced by the kinetic behavior of drops on the Cu/CuO@PFDTCS micropillar arrays. Compared to the arrays with a bigger D_{pillar} of 300 μm, the lateral and vertical deformations of the HTPB drops are small on the arrays with a D_{pillar} of 100 μm while laterally moving the arrays beneath the drops and lifting the drops vertically from the surface (Supplementary Movies S2 and S3). The smaller the deformation is, the smaller the adhesion force is. In addition, no observable lateral and vertical deformations of the glycerol drop could be detected while moving the arrays ($D_{pillar} = 100\,\mu m$) beneath the drops and lifting the drops vertically from the surface (Supplementary Movies S4 and S5). However, small deformations were detected in the case of water. This difference proved that glycerol with higher viscosity has smaller adhesion force with the arrays compared to water. Furthermore, the smaller deformation of glycerol than HTPB on the arrays ($D_{pillar} = 100\,\mu m$) demonstrated that higher surface tension can reduce the adhesion force (Supplementary Movie S6).

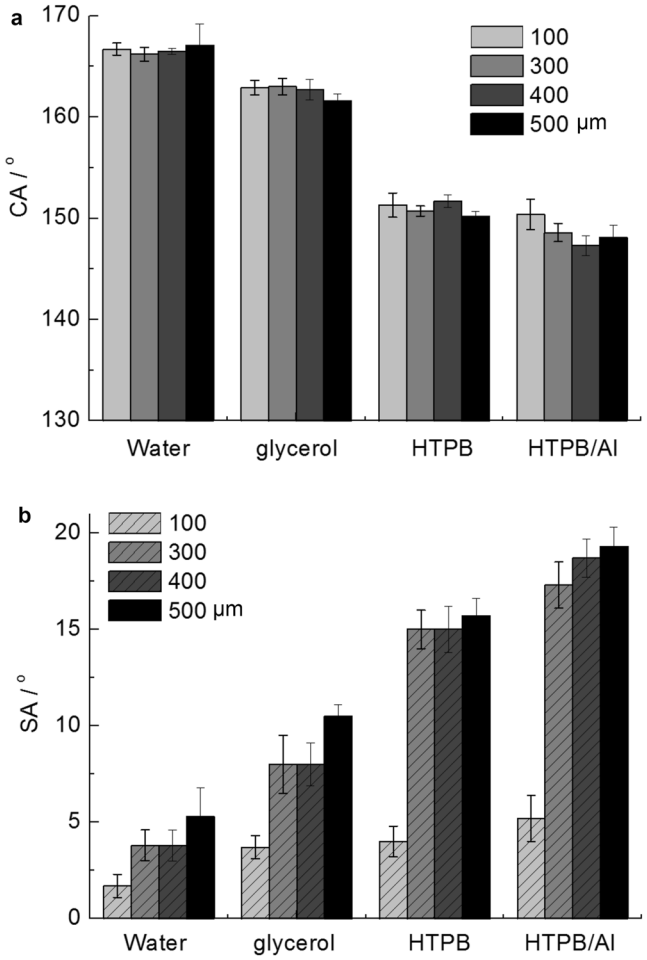

Figure 5. Effect of D_{pillar} on superamphiphobicity. (**a**) CAs and (**b**) SAs of water, glycerol, HTPB and HTPB/Al on the surface of the Cu/CuO@PFDTCS micropillar arrays with different D_{pillar}.

We also studied the kinetic interaction of the Cu/CuO@PFDTCS micropillar arrays with various liquids by checking whether there were residuals on the micropillar arrays after the drop rolled off the surfaces (Table 4). For water and glycerol, no visible liquid "left behind" was observed on all the arrays after the drops rolled off the surfaces. The depinning at the receding edge of the drops was fast and complete. For viscous HTPB, no residual was found on the arrays with a D_{pillar} of 100 μm, whereas residuals were detected on the arrays with bigger D_{pillar}. The residuals of HTPB/Al were apparent on all the arrays. The formation of these residual microdrops arises from microcapillary bridge rupture that occurs during receding events[43]. McCarthy *et al.* verified the conjecture concerning microcapillary bridge rupture using a non-volatile ionic liquid, which was observed via SEM on the staggered rhombus posts of a superhydrophobic surface[43]. We *in situ* observed the process of microcapillary bridge rupture for the first time using highly viscous liquids (HTPB and HTPB/Al) by laterally moving the arrays beneath the drops (Fig. 7 and Supplementary Movie S7). The process of microcapillary bridge rupture is more obvious for HTPB/Al owing to its high viscosity.

Rolling of various liquids on Cu/CuO@PFDTCS micropillar arrays. Once the gravitational force acting on a sessile liquid drop on a tilted surface overcomes the lateral adhesion force, the drop starts rolling[27]. The rolling velocity of liquid drops on super anti-wetting surfaces is relevant for their diverse applications, such as self-cleaning, anti-icing and microfluidics, etc[27]. Thus, the kinetic interaction of the Cu/CuO@PFDTCS micropillar arrays with various liquids was further studied by recording the rolling velocity of various liquids on the arrays. The motion of liquid drops (20 μL) on the 15° tilted Cu/CuO@PFDTCS micropillar arrays was filmed (Supplementary Fig. S5), and the velocity was calculated as shown in Table 5. In the rolling process, the potential energy of drops was only partially converted to kinetic energy because of energy loss. The energy loss in the course of rolling on solid surfaces arises mainly from viscous dissipation and surface adhesion[47]. Water drops rolled off the arrays (20 mm) very fast, and it is difficult to record the time (~0.2 s) accurately using a normal video camera (25 fps). No obvious influence of the D_{pillar} on the velocity was found. The velocity of glycerol is lower than that of water as shown in Supplementary Movie S8 because of it high viscosity, causing viscous dissipation in the rolling process. For glycerol, the contribution of surface adhesion to energy loss should be smaller than that of water, as the adhesion forces are smaller for glycerol on the same arrays. With increasing viscosity and decreasing surface tension of the liquids, the rolling velocity became even lower on all the arrays. For example, the velocity of HTPB

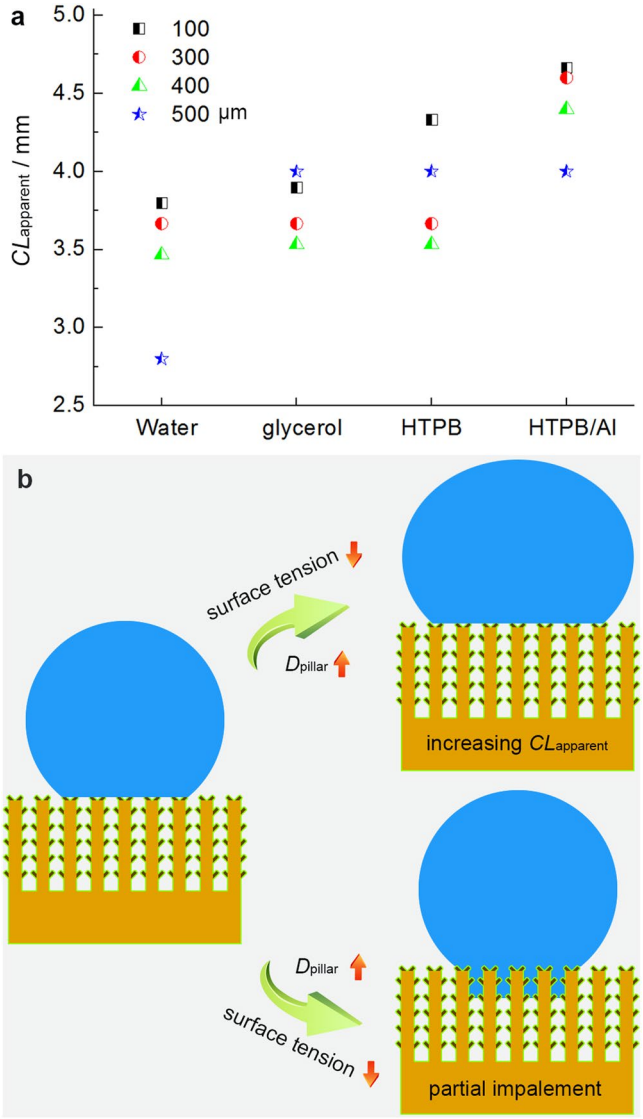

Figure 6. Liquid-solid interaction. (**a**) $CL_{apparent}$ of various liquids on the surface of the Cu/CuO@PFDTCS micropillar arrays. (**b**) Schematic illustration of two possible approaches that the Cu/CuO@PFDTCS micropillar arrays support the liquids with changing the D_{pillar} and the surface tension.

Adhesion forces/μN	D_{pillar}/μm			
	100	300	400	500
Water	32.4	87.3	86.3	84.3
Glycerol	23.6	75.5	69.5	75.5
HTPB	34.3	116.7	108.9	106.9
HTPB/Al	52.0	91.2	95.2	75.5

Table 3. Adhesion forces. Adhesion forces between the Cu/CuO@PFDTCS micropillar arrays and various liquids.

is 0.44 mm s^{-1} and the velocity of HTPB/Al is 0.26 mm s^{-1} on the arrays with a D_{pillar} of 100 μm. This is owing to the increase of both viscous dissipation (higher viscosity as shown in Table 1) and surface adhesion (higher adhesion force as shown in Table 3). In addition, it was found that the D_{pillar} also has big influence on the rolling velocity (Supplementary Movie S9). The arrays with a D_{pillar} of 100 μm exhibited the highest velocity among all the arrays for glycerol, HTBP and HTBP/Al. This is attributed to the smallest adhesion forces on the arrays with a D_{pillar} of 100 μm. The above results indicate that it is possible to enhance the rolling velocity of viscous liquids by reducing the adhesion force at the solid-liquid interface and by reducing the viscosity of the liquids.

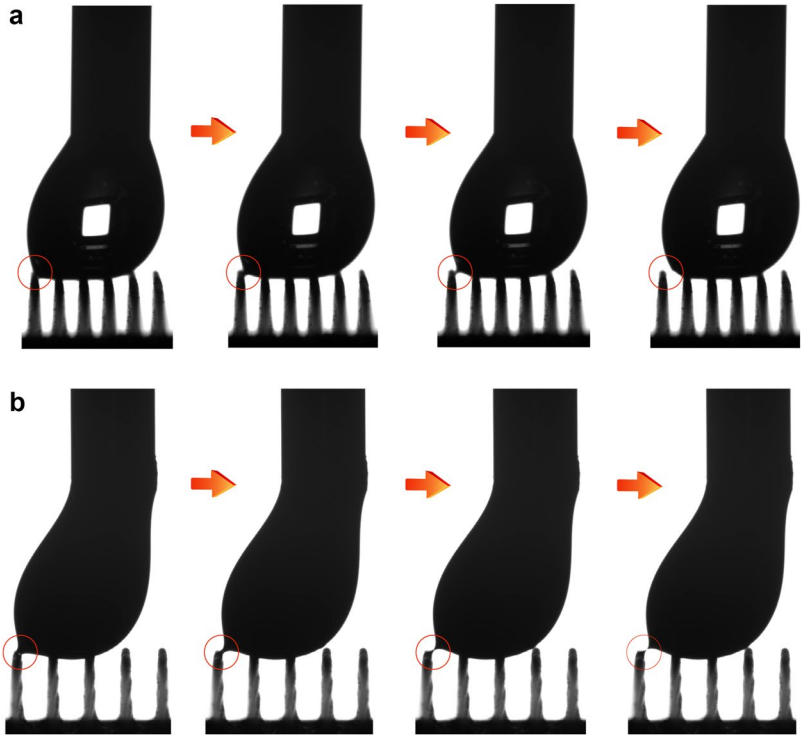

Figure 7. Microcapillary bridge rupture. *In situ* observation of microcapillary bridge rupture on the Cu/CuO@PFDTCS micropillar arrays using (**a**) HTPB ($D_{pillar} = 300\,\mu m$) and (**b**) HTPB/Al ($D_{pillar} = 500\,\mu m$) as the probing liquids (10 μL).

Residuals	D_{pillar}/μm			
	100	300	400	500
Water	No	No	No	No
Glycerol	No	No	No	No
HTPB	No	Yes	Yes	Yes
HTPB/Al	Yes	Yes	Yes	Yes

Table 4. Liquid-solid interaction. Summaries of residuals or not on the Cu/CuO@PFDTCS micropillar arrays after the drops of various liquids rolled off. "No" means no residual, and "Yes" means residual was observed.

Average rolling velocity/(mm s^{-1})	D_{pillar}/μm			
	100	300	400	500
Water	100	100	100	100
Glycerol	24.39	6.90	5.04	3.66
HTPB	0.44	0.23	0.20	0.19
HTPB/Al	0.26	0.15	0.14	0.11

Table 5. Average rolling velocity. Average rolling velocity of various liquids (20 μL) on the 15° tilted Cu/CuO@PFDTCS micropillar arrays.

Discussion

Superamphiphobic surfaces with high repellency towards liquids of extremely high viscosity and low surface tension were prepared. The contact angles, sliding angles, apparent contact line at the solid-liquid interface and adhesion forces of the superamphiphobic surfaces depend on micropillar distance, viscosity and surface tension of the liquids. Smaller micropillar distance, higher viscosity and higher surface tension are helpful to reduce the adhesion force. The process of microcapillary bridge rupture at the solid-liquid interface was *in situ* observed for the first time by using highly viscous liquids. Also, the adhesion forces were reduced, and the rolling velocity of liquids of extremely high viscosity and low surface tension was enhanced by reducing the micropillar distance. The superamphiphobic surfaces may find applications in many fields, especially in the conditions encountering viscous liquids of low surface tension. We believe that the results in this study will shed a light on the design of

novel superamphiphobic surfaces with high repellency towards complex liquids. Also, we should pay much attention to the kinetic wettability of super anti-wetting surfaces besides the static wettability.

Experimental Section

Materials. The Cu micropillar arrays (2 × 2 cm) with the same pillar size (200 × 200 μm) and different micropillar distance (D_{pillar} = 100, 300, 400 and 500 μm) were prepared by Institute of Chemical Materials, China Academy of Engineering Physics. HCl (37%), NaOH, ammonium persulfate, CTAB, toluene, glycerol and ethanol were purchased from China National Medicines Co. Ltd. PFDTCS (97%) was purchased from Gelest. HTPB with an average molecular weight of 3000 was supplied by China Haohua Chemical Group Co., Ltd. Al powder (100 μm) was supplied by Angang Group Aluminium Powder Co., Ltd.

Preparation of micro-/nanostructured Cu/CuO micropillar arrays. The micro-/nanostructured Cu/CuO micropillar arrays were prepared by modifying a previously reported method[52,53]. First, the Cu micropillar arrays were ultrasonicated for 30 min in water, and then immersed in 0.1 M HCl aqueous solution for 30 s to dissolve the oxides on the surface. The arrays were then rinsed with deionized water, and dried under a nitrogen flow. Subsequently, the Cu micropillar arrays were oxidized in 200 mL of an aqueous solution containing 5 M NaOH and 0.3 M ammonium persulfate at room conditions for 2 h. In this step, the nanostructured CuO layer was grown on the micropillar arrays. The as-prepared Cu/CuO micropillar arrays were rinsed with deionized water, and then dried under a nitrogen flow.

Preparation of superamphiphobic Cu/CuO@PFDTCS micropillar arrays. The micro-/nanostructured Cu/CuO micropillar arrays were immersed in 150 mL of dry toluene, and then 40 μL of PFDTCS was added. The sample was kept in the above solution for 12 h at room temperature to ensure complete modification of the CuO layer. The as-prepared Cu/CuO@PFDTCS micropillar arrays were washed with 20.0 mL of dry toluene and dried under a nitrogen flow.

Measurement of wettability. The CAs and SAs of the probing liquids were measured on a Contact Angle System OCA20 (Dataphysics, Germany) equipped with a tilting table. The syringe was positioned in a way that the liquid drops (20 μL) could contact surface of the samples before leaving the needle. It should be noted that the HTPB and HTPB/Al drops of smaller size are difficult to be dropped onto the surfaces because of their very high viscosity. We measured the CA of water and *n*-hexadecane using drops of different volumes (Supplementary Table S1). We found that the drop volume has very small influence on the CA measurements on surface of the superamphiphobic Cu/CuO@PFDTCS micropillar arrays. Tilting angle of the table was adjustable (0°–70°), and the subsequent measurement of the SAs was allowed at the same position on the sample. The rolling velocity was measured using a timekeeper while moving of a liquid drop on the 15° tilted surface. A minimum of six readings were recorded for each sample, and the average values with standard errors were reported.

Measurement of adhesion forces. The interfacial adhesive forces between the liquids and the surfaces were measured using a Force Tensiometer K100 (Krüss, Germany) at room temperature. The surface was placed on the balance table and moved upward at a constant speed of 3 mm min^{-1} until it contacted the probing liquid drop suspended with a copper ring, and continuously moved upward for 0.5 mm. Then, the surface was moved downward at a constant speed of 1 mm min^{-1} until the sample broke away from the drop.

Characterization. The micrographs of the samples were taken using SEM (CamScan Apollo300). Before SEM observation, all samples were fixed on Al stubs and coated with gold (~7 nm). The XPS spectra of samples were obtained using a VG ESCALAB 250 Xi spectrometer equipped with a monochromated Al Kα X-ray radiation source and a hemispherical electron analyzer. The spectra were recorded in the constant pass energy mode with a value of 100 eV, and all binding energies were calibrated using the C 1s peak at 284.6 eV as the reference. Viscoelastic properties of the probing liquids were recorded using a rheometer (Anton Paar Physica, MCR102) at 20 °C. The shear rate was set to be increased from 0.1 to 100 s^{-1} during the test. The changes in the shear stresses with the shear rates were recorded by the software of the rheometer. The surface tension of the liquids was measured using a Force Tensiometer K100 (Krüss, Germany) at 20 °C. The density of the liquids was measured using a previously reported method[47].

References

1. Barthlott, W. & Neinhuis, C. Purity of the sacred lotus, or escape from contamination in biological surfaces. *Planta* **202**, 1–8 (1997).
2. Neinhuis, C. W. B. Characterization and distribution of water-repellent, self-cleaning plant surfaces. *Ann. Bot.* **79**, 667–677 (1997).
3. Azimi, G., Dhiman, R., Kwon, H.-M., Paxson, A. T. & Varanasi, K. K. Hydrophobicity of rare-earth oxide ceramics. *Nat. Mater.* **12**, 315–320 (2013).
4. Bhushan, B. & Jung, Y. C. Natural and biomimetic artificial surfaces for superhydrophobicity, self-cleaning, low adhesion, and drag reduction. *Prog. Mater. Sci.* **56**, 1–108 (2011).
5. Liu, Y. *et al*. Pancake bouncing on superhydrophobic surfaces. *Nat. Phys.* **10**, 515–519, https://doi.org/10.1038/nphys2980 (2014).
6. Chu, Z. & Seeger, S. Superamphiphobic surfaces. *Chem. Soc. Rev.* **43**, 2784–2798 (2014).
7. Bellanger, H., Darmanin, T., de Givenchy, E. T. & Guittard, F. Chemical and physical pathways for the preparation of superoleophobic surfaces and related wetting theories. *Chem. Rev.* **114**, 2694–2716 (2014).
8. Tuteja, A. *et al*. Designing superoleophobic surfaces. *Science* **318**, 1618–1622 (2007).
9. Artus, G. R. J. *et al*. Silicone nanofilaments and their application as superhydrophobic coatings. *Adv. Mater.* **18**, 2758–2762 (2006).
10. Chu, Z., Feng, Y. & Seeger, S. Oil/water separation with selective superantiwetting/superwetting surface materials. *Angew. Chem. Int. Ed.* **54**, 2328–2338 (2015).
11. Wang, B., Liang, W. X., Guo, Z. G. & Liu, W. M. Biomimetic super-lyophobic and super-lyophilic materials applied for oil/water separation: a new strategy beyond nature. *Chem. Soc. Rev.* **44**, 336–361 (2015).
12. Zhang, F. *et al*. Corrosion resistance of superhydrophobic layered double hydroxide films on aluminum. *Angew. Chem. Int. Ed.* **47**, 2466–2469 (2008).

13. Zang, D. M. *et al*. Corrosion-resistant superhydrophobic coatings on mg alloy surfaces inspired by lotus seedpod. *Adv. Funct. Mater.* **27**, 1605446 (2017).
14. Matsubayashi, T. *et al*. Integrated anti-icing property of super-repellency and electrothermogenesis exhibited by PEDOT:PSS/cyanoacrylate composite nanoparticles. *ACS Appl. Mater. Interfaces* **8**, 24212–24220 (2016).
15. Shen, Y. Z. *et al*. Anti-icing performance of superhydrophobic texture surfaces depending on reference environments. *Adv. Mater. Interfaces* **4**, 1700836 (2017).
16. Zhang, J. & Seeger, S. Polyester materials with superwetting silicone nanofilaments for oil/water separation and selective oil absorption. *Adv. Funct. Mater.* **21**, 4699–4704 (2011).
17. Li, S., Huang, J., Chen, Z., Chen, G. & Lai, Y. A review on special wettability textiles: theoretical models, fabrication technologies and multifunctional applications. *J. Mater. Chem. A* **5**, 31–55 (2017).
18. Gao, L. & McCarthy, T. J. A perfectly hydrophobic surface (θA/θR = 180/180). *J. Am. Chem. Soc.* **128**, 9052–9053 (2006).
19. Parbat, D., Gaffar, S., Rather, A. M., Gupta, A. & Manna, U. A general and facile chemical avenue for the controlled and extreme regulation of water wettability in air and oil wettability under water. *Chem. Sci.* **8**, 6542–6554 (2017).
20. Chen, S., Li, X., Li, Y. & Sun, J. Intumescent flame-retardant and self-healing superhydrophobic coatings on cotton fabric. *ACS Nano* **9**, 4070–4076 (2015).
21. Ge, D., Yang, L., Zhang, Y., Rahmawan, Y. & Yang, S. Transparent and superamphiphobic surfaces from one-step spray coating of stringed silica nanoparticle/sol solutions. *Part. Part. Syst. Char.* **31**, 763–770 (2014).
22. Deng, X., Mammen, L., Butt, H. J. & Vollmer, D. Candle soot as a template for a transparent robust superamphiphobic coating. *Science* **335**, 67–70 (2012).
23. Liu, T. Y. & Kim, C. J. Turning a surface superrepellent even to completely wetting liquids. *Science* **346**, 1096–1100 (2014).
24. Song, M. R. *et al*. Controlling liquid splash on superhydrophobic surfaces by a vesicle surfactant. *Science Adv.* **3**, 1602188 (2017).
25. Maitra, T. *et al*. On the nanoengineering of superhydrophobic and impalement resistant surface textures below the freezing temperature. *Nano Lett.* **14**, 172–182 (2014).
26. Teisala, H. *et al*. Ultrafast processing of hierarchical nanotexture for a transparent superamphiphobic coating with extremely low roll-off angle and high impalement pressure. *Adv. Mater.* **30**, e1706529 (2018).
27. Gao, N. *et al*. How drops start sliding over solid surfaces. *Nat. Phys.* **14**, 191 (2017).
28. Fernandes, H. C. M., Vainstein, M. H. & Brito, C. Modeling of droplet evaporation on superhydrophobic surfaces. *Langmuir* **31**, 7652–7659 (2015).
29. Li, B., Yao, Z. & Hao, P. Incompressible LBGK simulation of flow characteristics in a micro-channel with patterned superhydrophobic surfaces. *Appl. Math. Model.* **39**, 300–308 (2015).
30. Peng, C., Chen, Z. & Tiwari, M. K. All-organic superhydrophobic coatings with mechanochemical robustness and liquid impalement resistance. *Nat. Mater.* **17**, 355–360 (2018).
31. Li, B. & Zhang, J. Durable and self-healing superamphiphobic coatings repellent even to hot liquids. *Chem. Commun.* **52**, 2744–2747 (2016).
32. Tian, X., Verho, T. & Ras, R. H. A. Moving superhydrophobic surfaces toward real-world applications. *Science* **352**, 142–143 (2016).
33. Yu, S., Guo, Z. & Liu, W. Biomimetic transparent and superhydrophobic coatings: from nature and beyond nature. *Chem. Commun.* **51**, 1775–1794 (2015).
34. Zhang, J., Yu, B., Gao, Z., Li, B. & Zhao, X. Durable, transparent, and hot liquid repelling superamphiphobic coatings from polysiloxane-modified multiwalled carbon nanotubes. *Langmuir* **33**, 510–518 (2017).
35. Zhou, H. *et al*. A Waterborne coating system for preparing robust, self-healing, superamphiphobic surfaces. *Adv. Funct. Mater.* **27**, 1604261 (2017).
36. Zhang, J., Gao, Z., Li, L., Li, B. & Sun, H. Waterborne nonfluorinated superhydrophobic coatings with exceptional mechanical durability based on natural nanorods. *Adv. Mater. Interfaces* **4**, 1700723 (2017).
37. Mates, J. E., Bayer, I. S., Palumbo, J. M., Carroll, P. J. & Megaridis, C. M. Extremely stretchable and conductive water-repellent coatings for low-cost ultra-flexible electronics. *Nat. Commun.* **6**, 8874 (2015).
38. Wu, L., Li, L., Li, B., Zhang, J. & Wang, A. Magnetic, durable, and superhydrophobic polyurethane@Fe_3O_4@SiO_2@fluoropolymer sponges for selective oil absorption and oil/water separation. *ACS Appl. Mater. Interfaces* **7**, 4936–4946 (2015).
39. Wong, W. S. Y. *et al*. Mimosa Origami: A nanostructure-enabled directional self-organization regime of materials. *Science Adv.* **2**, e1600417 (2016).
40. Jokinen, V., Kankuri, E., Hoshian, S., Franssila, S. & Ras, R. H. A. Superhydrophobic blood-repellent surfaces. *Adv. Mater.* 1705104 (2018).
41. Popova, A. A. *et al*. Droplet-array (DA) sandwich chip: a versatile platform for high-throughput cell screening based on superhydrophobic–superhydrophilic micropatterning. *Adv. Mater.* **27**, 5217–5222 (2015).
42. Wallace, R. A. *et al*. Superhydrophobic analyte concentration utilizing colloid-pillar array SERS substrates. *Anal. Chem.* **86**, 11819–11825 (2014).
43. Krumpfer, J. W., Bian, P., Zheng, P., Gao, L. & McCarthy, T. J. Contact angle hysteresis on superhydrophobic surfaces: an ionic liquid probe fluid offers mechanistic insight. *Langmuir* **27**, 2166–2169 (2011).
44. Quéré, D. Ra. D. Viscous drops rolling on a tilted non-wettable solid. *J. Colloid Interface Sci.* **48**, 286–291 (1999).
45. Zhao, B. Y., Wang, X., Zhang, K., Chen, L. Q. & Deng, X. Impact of viscous droplets on superamphiphobic surfaces. *Langmuir* **33**, 144–151 (2017).
46. Raiyan, A., McLaughlin, T. S., Annavarapu, R. K. & Sojoudi, H. Effect of superamphiphobic macrotextures on dynamics of viscous liquid droplets. *Sci. Rep.* **8**, 15344 (2018).
47. Khedir, K. R. *et al*. Temperature-dependent bouncing of super-cooled water on teflon-coated superhydrophobic tungsten nanorods. *Appl. Surf. Sci.* **279**, 76–84 (2013).
48. Brown, P. S. & Bhushan, B. Durable superoleophobic polypropylene surfaces. *Phil. Trans. R. Soc. A* **374**, 20160193 (2016).
49. Harrold, V. C., Paven, M., Vollmer, D. & Sharp, J. S. Rheological properties of viscoelastic drops on superamphiphobic substrates. *Langmuir* **32**, 4071–4076 (2016).
50. Li, L. X., Li, B. C. & Zhang, J. P. Dopamine-mediated fabrication of ultralight graphene aerogels with low volume shrinkage. *J. Mater. Chem. A* **4**, 512–518 (2016).
51. Zhang, J. & Seeger, S. Superoleophobic coatings with ultralow sliding angles based on silicone nanofilaments. *Angew. Chem. Int. Ed.* **50**, 6652–6656 (2011).
52. Zhang, W., Wen, X., Yang, S., Berta, Y. & Wang, Z. L. Single-crystalline scroll-type nanotube arrays of copper hydroxide synthesized at room temperature. *Adv. Mater.* **15**, 822–825 (2003).
53. Zhu, X. *et al*. Facile fabrication of a superamphiphobic surface on the copper substrate. *J. Colloid Interf. Sci.* **367**, 443–449 (2012).

Acknowledgements

We are grateful for financial support of the Presidential Foundation of China Academy of Engineering Physics (YZ2015010), the "Hundred Talents Program" of the Chinese Academy of Sciences, and the Funds for Creative Research Groups of Gansu, China (17JR5RA306).

Author Contributions

Q. Zhu, and B.C. Li performed the experimental design and data analysis, and wrote the manuscript; S.B. Li, G. Luo, B.H. Zheng performed the data analysis; J.P. Zhang performed the experimental design and data analysis, and contributed to writing the manuscript.

Additional Information

Supplementary information accompanies this paper at https://doi.org/10.1038/s41598-018-37368-y.

Competing Interests: The authors declare no competing interests.

Publisher's note: Springer Nature remains neutral with regard to jurisdictional claims in published maps and institutional affiliations.